JOURNAL OF GEOPHYSICAL RESEARCH: SOLID EARTH, VOL. 118, 1–10, doi:10.1029/2012JB009675, 2013

Rupture directivity of small earthquakes at Parkfield

Deborah L. Kane,[1,2] Peter M. Shearer,[1] Bettina P. Goertz-Allmann,[3,4] and Frank L. Vernon[1]

Received 2 August 2012; revised 5 November 2012; accepted 13 November 2012.

[1] Theoretical modeling of strike-slip ruptures along a bimaterial interface suggests that earthquakes initiating on the interface will have a preferred rupture direction. We test this model with 450 small earthquakes ($2 < M < 5$) from Parkfield, California, to look for evidence of consistent rupture directivity along the San Andreas Fault. We analyze azimuthal variations in earthquake source spectra after applying an iterative correction for wave propagation effects. Our approach avoids directly modeling source spectra because these models generally assume symmetric rupture; instead, we look for azimuthal variations in the amplitudes of the source spectra over specified frequency bands. Our overall results show similar proportions of events exhibiting characteristics of rupture directivity toward either the southeast or northwest. However, the proportion of events with southeast rupture directivity increases as we limit the data set to larger magnitudes, with 70% of the 46 events $M > 3$ exhibiting southeast rupture characteristics. Some spatial and temporal variability in rupture directivity is also apparent. We observe a higher proportion of northwest directivity ruptures following the 2004 M 6 Parkfield earthquake, which ruptured toward the northwest. Our results are generally consistent with the preferred southeast rupture directivity model but suggest that directivity is likely due to several contributing factors.

Citation: Kane, D. L., P. M. Shearer, B. P. Goertz-Allmann, and F. L. Vernon (2013), Rupture directivity of small earthquakes at Parkfield, *J. Geophys. Res. Solid Earth*, *118*, doi:10.1029/2012JB009675.

1. Introduction

[2] Fault rupture during an earthquake does not occur instantaneously. Rupture propagates from a site of nucleation with rupture velocities commonly estimated to be a substantial fraction of the shear wave velocity. When rupture propagates predominately in a single direction from nucleation, the resulting ground motion can be subject to dramatic azimuthal effects [*Ben-Menahem*, 1961].

[3] Commonly used models for small earthquake sources often assume simple radially symmetric rupture at a constant rupture velocity without allowing for more complex rupture propagation (e.g., expanding circular crack model and variations described by *Eshelby* [1957], *Brune* [1970], and *Madariaga* [1976]). However, observations of large earthquakes have shown that ruptures often propagate asymmetrically [*McGuire et al.*, 2002]. Several seismological studies have analyzed rupture propagation with respect to hypocenter location and have established the predominance of unilateral rupture propagation for large earthquakes [e.g., *McGuire et al.*, 2002; *Henry and Das*, 2001; *Mai et al.*, 2005]. Rupture propagation of smaller earthquakes, however, is much more difficult to observe due to insufficient seismic data resolution and azimuthal coverage; definitive observations of unilateral rupture propagation are limited [e.g., *Domanski et al.*, 2002; *Boatwright*, 2007]. Source property variations of such small events are more commonly treated with radially symmetric source models [e.g., *Allmann and Shearer*, 2007].

[4] One hypothesized mechanism of unilateral rupture propagation is due to the presence of a bimaterial interface at the fault, where two blocks of different rheological properties are positioned adjacently due to long-term slip. In some theoretical models of shear (mode II) ruptures along a bimaterial interface, slip occurs as asymmetric ruptures with a preferred rupture direction controlled by the properties of the two blocks [e.g., *Shi and Ben-Zion*, 2006]. Similar models incorporating different assumptions produce bilateral ruptures (e.g., *Andrews and Harris* [2005]; see *Yamashita* [2009] for an extensive discussion of model differences). Whether such a bimaterial model applies to the three-dimensional interfaces of natural faults has yet to be conclusively determined. Some researchers have argued that this model does not apply to natural faults because of the fault geometry and that localized stress heterogeneities will exert greater control over rupture propagation [*Harris and Day*, 2005, and references therein]. Earthquake relocation studies have produced much more clearly defined faults highlighted by

[1]Cecil H. and Ida M. Green Institute of Geophysics and Planetary Physics, Scripps Institution of Oceanography, University of California, San Diego, La Jolla, California, USA.
[2]Now at Department of Earth Sciences, University of New Hampshire, Durham, New Hampshire, USA.
[3]ETH Zurich, Institute of Geophysics / Schweizer. Erdbebendienst, Sonneggstrasse, Zurich, Switzerland.
[4]Now at NORSAR Kjeller, Norway.

Corresponding author: D. L. Kane, Department of Earth Sciences, University of New Hampshire, 56 College Rd., Durham, NH 03824-2601 USA. (deborah.kane@unh.edu)

2169-9313/13/2012JB009675

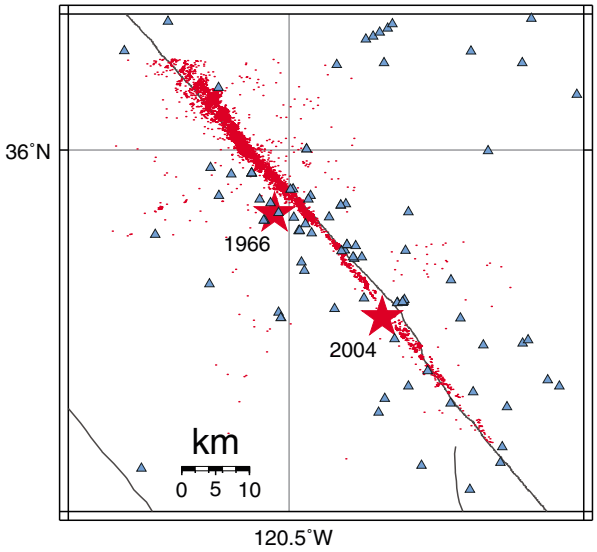

Figure 1. Stations (triangles) and earthquakes (dots) along the Parkfield segment of the San Andreas Fault (SAF) used in this analysis. The locations of the 1966 and 2004 *M* 6 events are indicated with stars.

locations of smaller earthquakes [e.g., *Thurber et al*., 2006; *Lin et al*., 2007], but whether these faults can be adequately modeled by a planar surface or whether a more complex geometry is dominant remains unclear.

[5] The San Andreas Fault (SAF) at Parkfield, California, is a close natural approximation to a bimaterial interface. The seismicity along the fault is distributed along a vertical plane (Figure 1) and previous studies at Parkfield concluded that the fault represents a distinct, natural barrier between blocks of different characteristics [*Eberhart-Phillips and Michael*, 1993; *Thurber et al*., 2006; *Zhao et al*., 2009]. Applying the asymmetric rupture model [e.g., *Shi and Ben-Zion*, 2006] to this region of the SAF by considering the fault as a barrier between two single blocks predicts a preferred rupture direction along the fault strike toward the southeast [*Ben-Zion*, 2006]. The SAF is therefore a good candidate fault for testing whether the computational model is applicable to the complex three-dimensional structure exhibited in real faults, and for determining if this model offers an explanation for variability in rupture direction. The observation of a preferred rupture direction and the subsequent effects on ground motion would have widespread implications for both earthquake source physics and for earthquake hazard analysis on mature faults because ground motion amplified by unilateral rupture directivity could produce greater damage than might otherwise be expected.

[6] The SAF at Parkfield had its long-awaited *M* 6 earthquake in September 2004 after 38 years following the previous 1966 *M* 6 earthquake. This recent large event at Parkfield sparked considerable interest and debate in the bimaterial interface model. *Harris and Day* [2005] reviewed studies of prior *M* 4 to 6 earthquakes at Parkfield and summarized the rupture directions of this set of events: the two previous *M* 6 Parkfield earthquakes in 1934 and 1966 ruptured toward the southeast and matched the prediction of the bimaterial interface model, but five *M* 4 to 5 events did not match the prediction. The 2004 event nucleated near the southeast end of the Parkfield section and propagated toward the northwest [*Bakun et al*., 2005; *Langbein et al*., 2005; *Fletcher et al*., 2006]. *Harris and Day* [2005, 2006] presented this observational evidence along with a review of numerical simulations and concluded that the bimaterial interface was likely not the primary effect controlling rupture direction. A subsequent comment by *Ben-Zion* [2006] attributed the earthquake nucleation to a subfault and suggested that the rupture direction matched the preferred direction for this subfault. The SAF at Parkfield has been extensively studied, but it is clear that the complexities of the fault either obscure a rupture directivity preference due to smaller scale structure or allow other effects to control rupture direction.

[7] Additional studies of smaller earthquakes at Parkfield have contributed further to this debate through observations of asymmetric distributions of small earthquake locations [*Rubin and Gillard*, 2000; *Rubin*, 2002] and asymmetric aftershock locations [*Zaliapin and Ben-Zion*, 2011]. A recent study [*Lengliné and Got*, 2011] used repeating earthquake sequences (*M* 1.0 to 3.2) to observe a predominance of southeast rupture propagation in the region of the fault with the largest velocity contrasts across the fault boundary. Another study [*Wang and Rubin*, 2011] estimated rupture directivity of earthquakes (*M* 0.5 to 3.0) at Parkfield by modeling synthetic spectral ratios and found that of the best-resolved events, ~40% exhibited bilateral rupture characteristics and more than 80% of the remaining unilateral events showed southeast rupture directivity.

[8] In this study, we seek to constrain the presence or absence of a preferred rupture direction along the fault by studying small earthquakes at Parkfield while minimizing the analysis assumptions. We look for evidence that small ($M < 5$) earthquakes at Parkfield exhibit characteristics of unilateral rupture directivity along the strike of the fault. We do not use common point-source earthquake models in our analysis because such models generally assume symmetric rupture. Instead, we look for azimuthal differences in spectral amplitudes of *P*-wave displacement spectra to constrain the rupture direction. For a model earthquake with unilateral rupture directivity along the fault strike, we expect to see larger spectral amplitudes at higher frequencies in the direction of rupture and smaller spectral amplitudes in the opposite direction. However, these directivity effects are easily masked by differences in the spectra caused by propagation path and station site effects, which are particularly strong at high frequencies. As a result, rupture directivity is usually difficult to resolve for individual earthquakes smaller than magnitude 3 to 4. Because these path effects are nearly the same among nearby earthquakes, directivity for small events can be resolved more reliably by comparing spectra among different events within spatially compact clusters and this is the approach we adopt here.

[9] By processing records from a large number of events, we are able to estimate empirical station and path correction terms for each cluster and isolate the source contributions. Azimuthal differences in the amplitudes of corrected spectra at a particular reference frequency can then be used to

estimate the significance and direction of any directivity signals. We obtain directivity signals for the majority of the 450 earthquakes that we analyze and compare these results with predictions of the bimaterial interface model.

2. Data: Parkfield Seismicity

[10] At Parkfield, a distinct section of the SAF is defined by boundaries separating the locked section toward the southeast from the creeping section toward the northwest [*Wallace*, 1990]. The recurrence of $M \sim 6$ earthquakes at Parkfield has led to extensive studies of local seismicity and fault structure. Earthquakes at Parkfield generally occur along a vertical plane [*Eberhart-Phillips and Michael*, 1993; *Thurber et al*., 2006].

[11] Application of various earthquake relocation techniques has produced detailed images of fine fault structure while highlighting relatively shallow (~5 km depth) earthquake clusters broadly distributed to the northwest and distinctly separate bands of seismicity at somewhat greater depths (5 to 12 km) to the southeast [*Waldhauser et al*., 2004; *Thurber et al*., 2006]. Seismicity appears to occur along a single plane at depth, but two surface traces have been observed and the exact connection to the structure at depth remains unclear [*Thurber et al*., 2006; *Simpson et al*., 2006].

[12] The fault divides blocks of varying seismic velocities. Past tomographic studies have quantified across-fault velocity variations with contrasts of up to ~5–20% [*Eberhart-Phillips and Michael*, 1993; *Thurber et al*., 2006]. Velocity heterogeneities along the strike of the fault are clearly present. A fault-zone head-wave study resolved sharp contrasts of 5–10% near the epicenter of the 1966 Parkfield earthquake but very little contrast near the epicenter of the 2004 Parkfield earthquake [*Zhao et al*., 2009].

[13] We use a dataset of 2263 earthquakes recorded at 108 stations in central California to look for evidence of rupture directivity of small earthquakes on the SAF at Parkfield (Figure 1). This waveform data set is from the Northern California Earthquake Data Center and represents a subset of earthquakes recorded from 1984 to 2005. We use earthquake locations used in *Allmann and Shearer* [2007], which were relocated using the shrinking box method of *Lin and Shearer* [2005]. *Allmann and Shearer* [2007] previously used this data set to investigate spatial variability in coseismic stress drop prior to and following the 2004 M 6 Parkfield earthquake. We use the multitaper displacement P-wave spectra computed by *Allmann and Shearer* [2007] over 1.28 s windows for 100 sps data, and we maintain their defined signal-to-noise ratio constraints. The full data set consists of 31,432 displacement spectra.

3. Methods

3.1. Iterative Separation of Source and Path Spectral Contributions

[14] The close spacing of events, combined with a wide range of source-station distances (<1 km to 100 km) and source-station azimuths in this data set, present an opportunity to separate the effects of seismic wave propagation from the signal of the seismic sources. We assume that the ray paths between each of two closely located earthquakes and a given station will be approximately identical [*Hartzell*, 1978]. Thus, any effects of scattering and attenuation will also be similar along these paths. This assumption can be extended to a cluster of events with similar hypocentral locations recorded by any station, as long as the separation distance between the sources and a given station is sufficiently large compared to the interevent separation distances of the cluster. We use these similarities to our advantage by employing an iterative separation process to identify and isolate contributions from the individual earthquake sources and from the path effects. Previous studies have used this technique to determine average path effects for correcting source spectra [e.g., *Warren and Shearer*, 2002; *Prieto et al*., 2004; *Shearer et al*., 2006].

[15] The spatial distribution of events in this region is not sufficiently small to approximate all events as being from a single source location, and we must divide the events spatially to meet the conditions of our assumptions. We use the k-means clustering algorithm [*Lloyd*, 1982] to split the cataloged events into twenty clusters based on hypocentral locations by minimizing the distance separating a given event hypocenter from the centroid of a cluster of events (Figure 2). We initiate the clustering routine with cluster centroids chosen from a trial clustering of a subset of the data. K-means clustering tends to produce clusters of similar spatial scale, and trials using different numbers of clusters do not noticeably change the results.

[16] We perform the iterative separation of average source, path, and residual effects for each cluster of events following the method described in *Prieto et al*. [2004]. This process results in decomposing each log-displacement frequency spectrum, u_{ij}, into three spectral components:

$$u_{ij}(f) = s_i(f) + p_j(f) + r_{ij}(f) \quad (1)$$

Here s_i represents the source spectrum for event i averaged over all stations; p_j represents the effects due to travel path, local site response, and instrument response averaged over all events at station j; and r_{ij} represents the residual spectrum for each record. The travel path terms between each cluster and a given station are similar for adjacent clusters. We remove the resulting path terms, p_j, from the recorded displacement spectra, u_{ij}, to correct the records for path effects and leave only the source and residuals for further analysis (hereafter referred to as 'corrected' displacement spectra). These corrected spectra should retain signals due to rupture directivity, unless all events in a cluster rupture in the same direction. In this case, the directivity signal would be nearly identical for all events and would largely be absorbed into the path and station terms; the remaining directivity signal would be either absent or randomly distributed among the events. However, because the directivity effect on the spectrum also depends upon corner frequency (which decreases with increasing event size), this canceling effect will be most complete for the smaller, more numerous earthquakes in our analysis, and we may nonetheless obtain reliable directivity results for the larger magnitude earthquakes.

3.2. Measuring Directivity

[17] Unilateral rupture directivity will produce earthquake source pulses and source spectra that vary with azimuth [*Ben-Menahem*, 1961]. This effect can be observed as shorter duration, higher amplitude source time functions in the

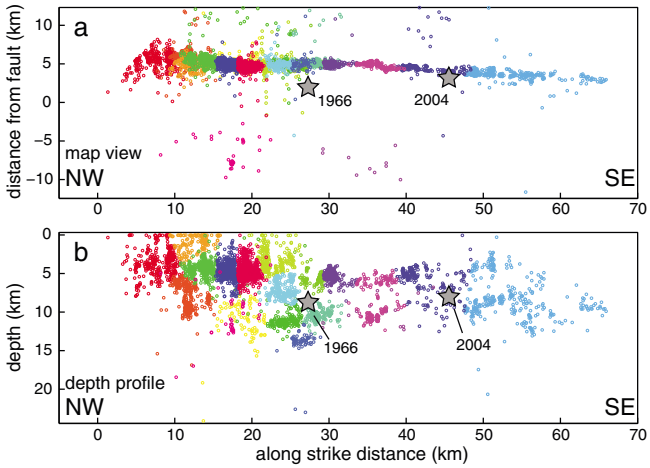

Figure 2. (a) Map view and (b) profile view of events considered in this study with spatial clustering indicated by color. The locations of the 1966 and 2004 events are included for reference.

direction of rupture, and longer duration, lower amplitude source time functions in the opposite direction. This dependence of duration on azimuth can be formulated using a simple model [e.g., *Haskell*, 1964] as

$$\tau(\theta) = \frac{L}{v_r} - \frac{L\cos\theta}{c} = \tau_0\left(1 - \frac{v_r}{c}\cos\theta\right). \quad (2)$$

Here τ represents the apparent duration of the source pulse and θ is the azimuth measured between the direction of rupture and the recording station. τ_0 is equivalent to the rupture length, L, divided by the rupture velocity v_r; this reference source pulse duration corresponds to the case where θ is zero or the rupture is bilateral. The seismic wave velocity is represented by c.

[18] In the frequency domain, this azimuthal variation appears as higher spectral amplitudes at higher frequencies in the direction of rupture and a lack of such high frequency signal in the opposite direction (Figure 3). Low frequency amplitudes of source spectra remain unchanged with azimuth. This effect on corner frequency is inversely related to the effect on source pulse duration and can be described by the azimuthal variation in apparent corner frequency of the source spectrum

$$f_{c,\mathrm{app}} = f_c \frac{1}{1 - \frac{v_r}{c}\cos\theta}. \quad (3)$$

Here the apparent corner frequency of the source spectrum $f_{c,\mathrm{app}}$, is a function of the true corner frequency, f_c, the rupture velocity, the seismic wave velocity, and the angle between the direction of rupture and the direction of the recording station. If we assume that each earthquake ruptures in a direction along the strike of the fault, then we can determine rupture direction by comparing the source spectra observed in each along-strike direction.

[19] We apply this concept to the Parkfield data set using the corrected *P*-wave displacement spectra for each cataloged earthquake. For each event, we select records from stations within a ±45° window of the SAF trace. The ±45° window will include apparent corner frequencies of ~$0.75f_c$ or less in the opposite direction of rupture, and ~$1.5f_c$ or greater in the direction of rupture (assuming a constant rupture velocity of 80% of the *S*-wave velocity and a *P*-wave velocity equivalent to $\sqrt{3}$ times the *S*-wave velocity). This window includes 180° of the total azimuthal directions, and preserves a large portion of the data for further analysis while assuring that several stations are likely to have adequate signal-to-noise ratios for each event. For each azimuthal window (to the southeast and to the northwest), we compute the mean corrected spectrum (Figure 4). We quantify the directivity as the log-difference of the mean spectral amplitude to the southeast direction and the mean spectral amplitude to the northwest direction over a specified frequency band (e.g., 15–20 Hz). This processing converts a set of spectra for each event into a single scalar value describing the rupture direction based on the assumptions of along-strike unilateral rupture. A positive value indicates higher average spectral amplitudes to the southeast while a negative value indicates higher average spectral amplitudes to the northwest. To obtain uncertainty estimates for these directivity measurements, we use

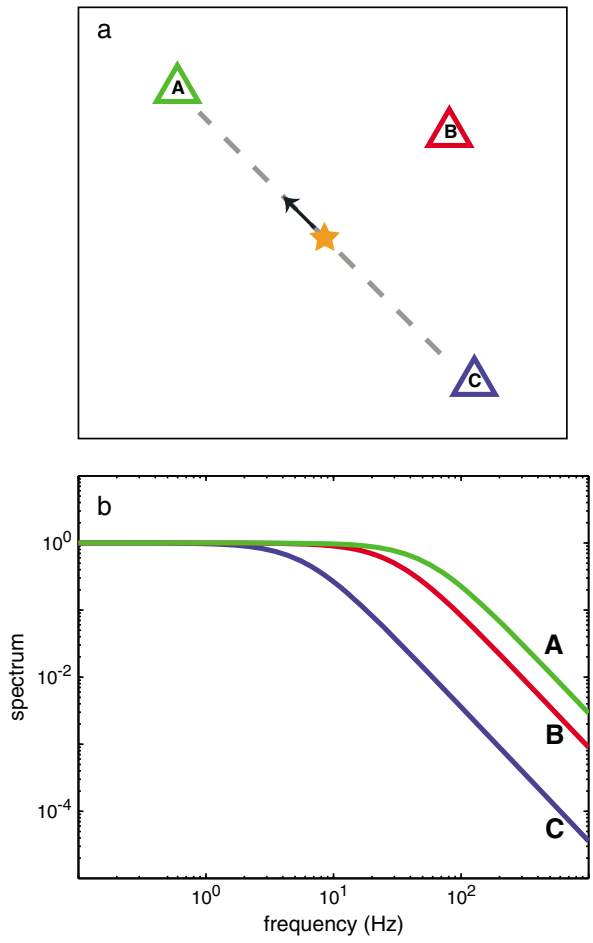

Figure 3. (a) Cartoon of earthquake rupture toward the northwest and (b) the resulting azimuthal behavior of the source spectra recorded by stations at various azimuths. Station coloring in Figure 3a indicates corresponding spectrum in Figure 3b.

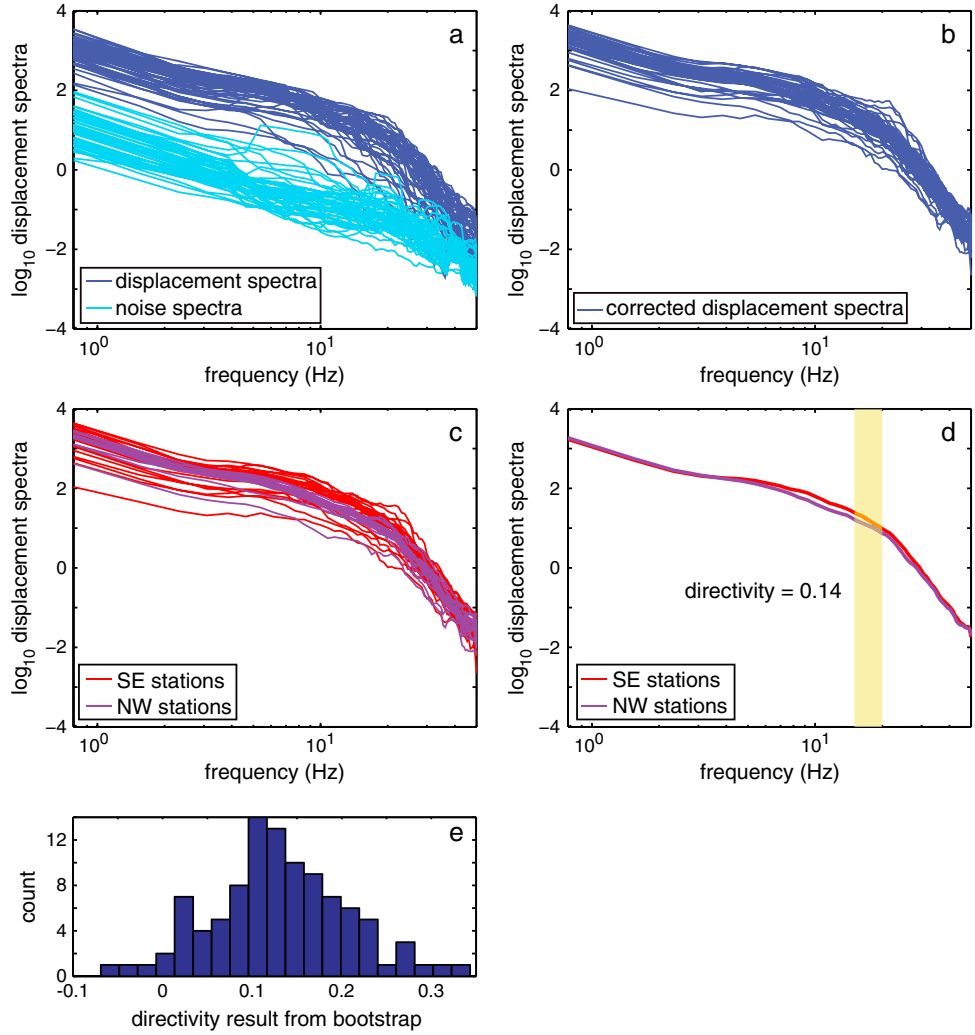

Figure 4. Example processing for an event. (a) Recorded displacement amplitude spectra (dark blue) are shown with noise spectra from time immediately preceding the *P*-wave arrival (light blue). (b) The spectra have been corrected by the iteratively computed path terms. (c) The spectra from stations falling within the defined azimuthal wedges from the event are color coded, with spectra recorded at stations to the southeast plotted in red and spectra recorded at stations to the northwest plotted in purple. (d) The mean spectrum in each of the two azimuthal wedges and highlight of the frequency band used to estimate the directivity. The positive directivity result indicates rupture directivity toward the southeast. (e) Histogram shows the distribution of directivity results obtained from bootstrap resampling; this event has a significant southeast directivity result because >90 out of 100 of the trial estimates produced a southeast directivity result.

statistical bootstrapping to resample the selection of spectra for each event 100 times with replacement. We consider the result to be significant if 90 or more of these estimates indicate the same rupture directivity (Figure 4).

[20] This method has a few limitations due to data availability and initial assumptions. We assume that unilateral rupture directivity will occur in a horizontal direction aligned with the trace of the fault. Any component of vertical rupture directivity or directivity misaligned from the fault strike will result in values that do not correspond with the true rupture direction. This method may not work well if there are too few records in either azimuthal direction because the averaging of the spectra may not result in sufficiently smooth spectra for measuring mean differences in spectral amplitudes. We limit our study to events with a minimum of three records toward the northwest and three records toward the southeast to minimize such effects.

[21] We use a single frequency band for analysis for earthquakes over a range of magnitudes, and the resulting directivity values will exhibit a dependence on magnitude because the true corner frequencies are related to magnitude (e.g., an M 4 event will have a higher directivity value than an M 3 event if all other conditions are equal because the true corner frequency of the M 4 event will be much lower than the band used to measure directivity). This effect can make it difficult to choose an appropriate frequency band to use for all events because the band needs to be beyond the corner frequencies of the events in order to resolve a separation of the spectra in each direction while staying within the limits of adequate signal-to-noise ratios.

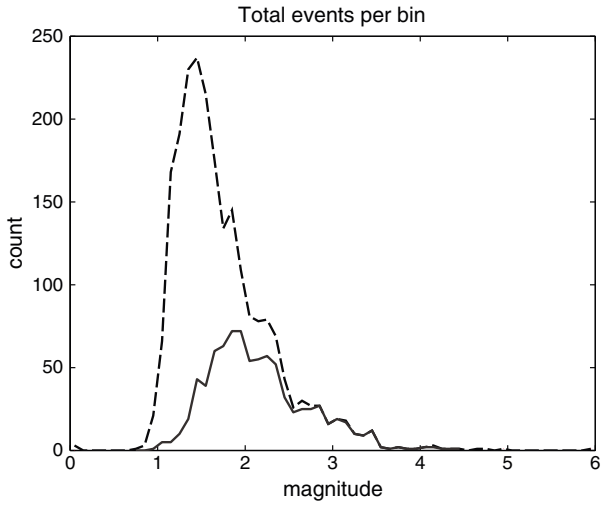

Figure 5. Distribution of events as a function of magnitude for all events tested (dashed line) and for all events meeting processing criteria and resulting in directivity estimates (solid line). Almost all events $M > 2.5$ produced directivity results, but events $M < 2$ rarely produced results. We define M 2 as a threshold for reliable results.

Variations in rupture velocity can also affect the resulting measurements because lower rupture velocities will produce smaller variations in corner frequency and directivity estimates at a given frequency band than would be expected at higher rupture velocities.

[22] Our method measures mean values of spectra and is appropriate to use in bands above the event corner frequencies. Because we limit our observations to a single frequency band, we are likely unable to resolve rupture directivity in events $M < 2$ for which the expected corner frequencies will be above our selected band (even when the directivity contribution is strong). We are limited in selection of higher frequency bands by the sampling rates of the data and by diminished signal-to-noise ratios. We confirm that the directivity value results are consistent across several frequency bands and not dependent on the band chosen for analysis by repeating our analysis using three different frequency bands of 5 Hz width (15 to 20 Hz, 20 to 25 Hz, and 25 to 30 Hz) and verifying that the results are consistent. In the following results, we focus on the 15 to 20 Hz band.

[23] Finally, recall that our method examines *relative* directivity signals among different events within compact event clusters and will work best if these clusters contain a mixture of unilateral ruptures in opposing directions. If all the events rupture in the same direction, then the directivity signal will be largely absorbed into the station and path terms in our spectral decomposition. In this case, the remaining directivity signal for events in the cluster would contain random fluctuations that could favor either rupture direction, which might lead us to falsely conclude that both rupture directions are present. We address this possibility in two ways. First, we perform statistical tests to verify that our inferred rupture directions are statistically significant with respect to random variations in the recording stations. Second, we compare the results obtained for larger magnitude events, for which the directivity signal is stronger and cannot be completely removed with the station and path corrections, with those for the smaller events.

4. Results

[24] Of the 2263 events ($1 < M < 5$) in our data set, 839 events met the minimum processing requirement of three records in each azimuthal wedge. The percentage of events meeting this criterion decreases rapidly for magnitudes below $M \sim 2$ (Figure 5). Results for the smallest events ($1 < M < 2$) show a slight preference for northwest directivity (53% of events); we note that these are likely poorly resolved and we do not include them in further analysis. The set of 450 earthquakes $2 < M < 5$ has similar proportions of events with directivity estimates toward the southeast and northwest. We observe 241 (54%) exhibiting rupture toward the southeast and 209 (46%) exhibiting rupture toward the northwest.

[25] The applied path correction between each cluster and each station removes the average propagation effects for the events in the cluster, but it does not account for any smaller scale propagation differences due to event location within a given cluster. We fit a simple one-dimensional along-strike model to the directivity results in each cluster to estimate a constant attenuation term (Q_P) for within the cluster. We do not estimate a frequency-dependent Q_P because the directivity results are measured over a narrow frequency band. Not all clusters show effects of local attenuation, and the estimates of Q_P range from ~70 to ~3000. Most Q_P values are consistent with the three-dimensional Q_P model presented by *Bennington et al*. [2008]; the higher values describe clusters with minimal trend in directivity estimates within the cluster. We apply the resulting attenuation corrections to the clusters. These corrections do not change the resulting rupture directivity in any of the events.

[26] We define a subset of our results for further analysis by selecting events in which the directivity to the northwest or southeast is significant at the 90% confidence level based on the uncertainty limits obtained with the bootstrap technique. It is important to note that a higher absolute value of directivity does not indicate a more significant result. Of these 243 significant events (54% of the total 450 directivity estimates), we find that 131 events (54%) exhibit southeast rupture and 112 events (46%) exhibit northwest rupture. These proportions change minimally if we decrease the significance cutoff to the 85% confidence level or if we increase the cutoff to the 95% confidence level, confirming that our results are robust. These results indicate that a preferred rupture direction does not seem to be a dominant effect overall in the seismogenic zone at Parkfield. We do not observe a strong preference for rupture direction over the full magnitude range considered, but it is necessary to further investigate characteristics of these events to find or rule out directivity on smaller spatial scales or over subsets of the data.

4.1. Effect of Location

[27] Figure 6 displays a map and profile view of the locations of these 243 significant events. Spatial variability in rupture direction is apparent, and rupture direction seems to show a preference within small groupings of event locations. These variations may represent true spatial differences in directivity properties related to smaller-scale rheological or stress variations along the fault.

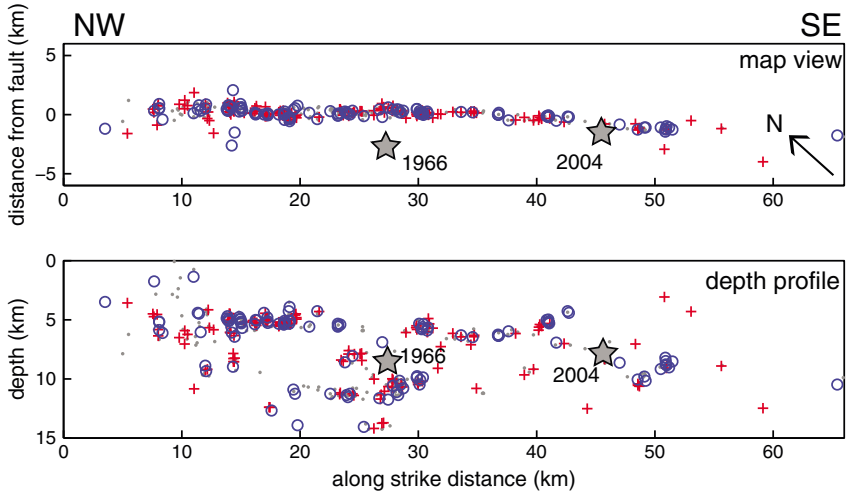

Figure 6. (a) Map and (b) profile views showing rupture directivity results. Events without significant results are indicated with a gray dot. Events with significant results are plotted as red 'plus' (SE rupture) and as blue 'open circle' (NW rupture).

[28] To confirm any true spatial variability in event rupture directivity, we first establish the independence of our results from the initial subgroups obtained in the clustering process. We investigate this visually by looking at the directivity results for individual clusters of events and comparing these with adjacent clusters. Within individual clusters, the directivity of events appears to be spatially grouped rather than randomly distributed. Because path corrections are uniformly applied to all events in each cluster and the interevent spacing differences are accounted for by the Q_P correction, such a signal is due to either inappropriate path corrections for some events or due to true variability in rupture directivity. Erroneous effects are also possible in the case where all events in a cluster rupture in the same direction, as discussed in consideration of the approach.

[29] We perform two simple tests to verify the independence of our results from the clustering process. First, we repeat the analysis using 30 smaller clusters instead of the initial 20. We find that the results of the overall data set change only minimally by decreasing the size of the clusters. Second, for two sets of adjacent clusters, we combine the adjacent clusters into a single larger cluster and repeat the analysis. We find that of the events processed in both the original 20 cluster analysis and in the combined clusters analysis, no events show a change in the rupture directivity result. These tests demonstrate that the spatial variability we observe in the rupture directivity results is not due to the clustering process and possibly represents true spatial variability in preferred rupture directivity.

4.2. Effect of the 2004 *M* 6 Parkfield Earthquake

[30] We compare the data from events prior to the 2004 *M* 6 earthquake with the data from events following the mainshock to determine if any rupture directivity preference exists that may be related to the interseismic period or to the aftershock sequence (Figure 7). The events prior to the 2004 earthquake exhibit a distribution of rupture direction similar to the overall data set, with 56% of events with significant unilateral directivity rupturing toward the southeast. Notably, the events following the 2004 earthquake exhibit a

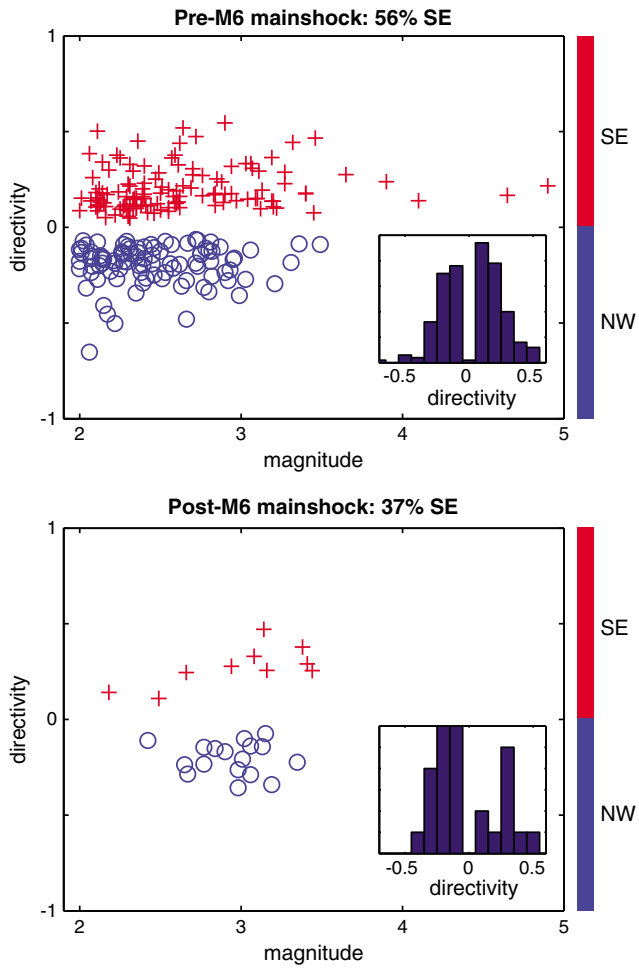

Figure 7. Comparison of directivity estimates for events prior to the 2004 *M* 6 mainshock with those following the mainshock; estimates are plotted by magnitude. Inset histograms show the overall distribution of estimates in each population. We observe a temporal change in the proportion of events with northwest rupture directivity.

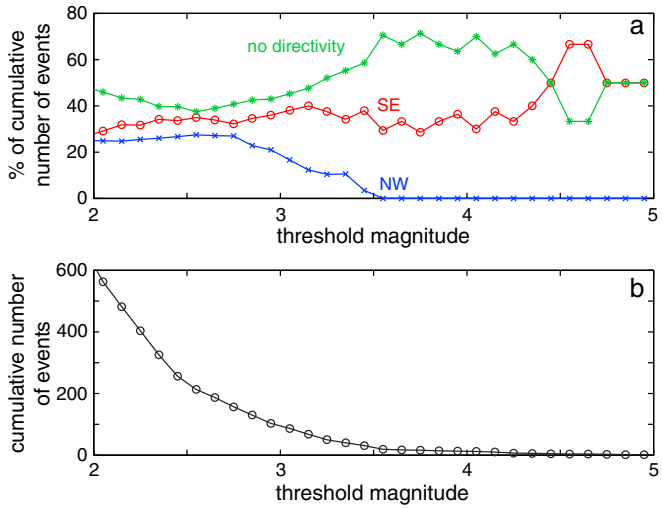

Figure 8. Percentage of results (a) above a given threshold magnitude exhibiting southeast rupture directivity (red line marked by 'o' symbols), northwest rupture directivity (blue line marked by 'x' symbols), or nonsignificant directivity results (green line marked by '*' symbols). (b), The total number of events considered at each threshold magnitude.

stronger preference for northwest directivity, with only 37% of events rupturing toward southeast and the remaining 63% toward northwest. The aftershocks seem to preferentially match the rupture direction of the mainshock, similar to comparisons of other mainshock source properties (e.g., focal mechanism orientation) with those of aftershocks. *Allmann and Shearer* [2007] used this data set to measure changes in attenuation following the 2004 mainshock. To test whether a coseismic attenuation change could be affecting our results, we perform a second set of attenuation corrections to allow for a change in local attenuation following the mainshock. We do not observe a significant difference in results when using a single attenuation correction for each cluster or separate time-dependent attenuation corrections.

4.3. Effect of Earthquake Magnitude

[31] Our method of measuring rupture directivity includes an inherent bias with event magnitude due to the limitations of using a single frequency band for all events. Smaller magnitude events will have higher spectral corner frequencies than larger magnitude events, and a smaller difference between southeast and northwest station spectra will subsequently occur. Because of this bias, it is necessary to consider the effects of earthquake magnitude on the results of the directivity estimates and to determine if any magnitude variation of directivity is due to the measurement bias or is a true difference among earthquake rupture size.

[32] Larger earthquakes are more likely to produce directivity estimates in our analysis because these events are generally recorded by more stations at greater distances and at higher signal-to-noise ratios than comparably located smaller earthquakes (Figure 5). The greater rupture area of larger magnitude events will also produce an effectively lower corner frequency in the source spectrum as compared to a smaller earthquake, and this effect will make the difference in spectral amplitudes greater at a given higher frequency than can be observed for a smaller earthquake. The effect of such difference is to obtain a higher number of significant directivity estimates for larger earthquakes. We do not observe a strong dependence of absolute value of directivity with magnitude as might be expected based on this bias (Figure 7).

[33] The proportion of events with southeast directivity increases relative to those with northwest directivity as larger magnitude earthquakes are considered (Figure 8). In Figure 9, we again plot the depth profile of events with significant results. We overlay this plot with a separate representation showing the rupture direction for events of magnitude greater than M 3. We observe a clear discrepancy in rupture directivity for events at these magnitudes. Instead of comparable proportions of events with rupture in either direction, we observe 70% of events with $M \geq 3$ exhibiting rupture toward the southeast and only 30% with rupture toward the northwest. This subset of data contains 46 events. Fourteen of these events occurred in the aftershock sequence of the 2004 M 6 Parkfield earthquake. For the events following the 2004 earthquake, 6 out of 14 exhibit rupture toward the southeast and the remaining 8 exhibit rupture toward the northwest.

5. Discussion and Conclusions

[34] We use a simple comparison of displacement spectra to estimate rupture directivity of small earthquakes at Parkfield. This method is best suited for cases of unilateral rupture directivity along the strike of the fault toward the northwest or the southeast, and cannot resolve rupture directivity in cases of bilateral rupture or for events without statistically significant rupture directivity results. A lack of available data with adequate frequency content or poor geographic distribution of stations can also obscure rupture directivity effects within the overall dataset. Although the effects of these limitations are important to consider for rupture directivity estimates of individual events, we expect this simple method to be sufficient when working with a large set of data.

[35] Our analysis considers 2263 events ($1 < M < 5$) at Parkfield and produces 450 directivity estimates ($2 < M < 5$) after removing events with insufficient azimuthal data coverage, applying corrections for propagation paths, applying

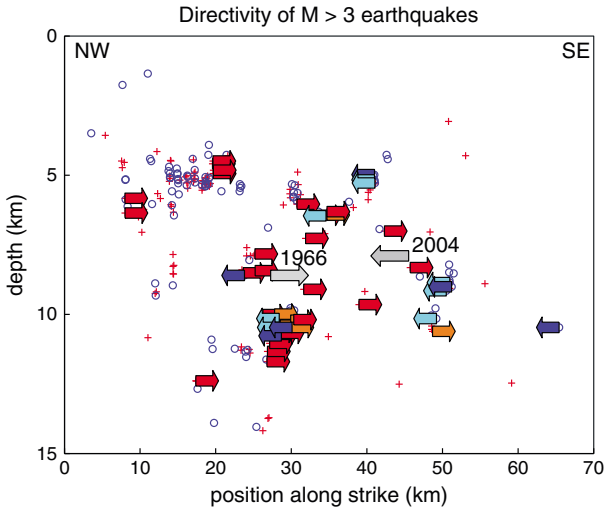

Figure 9. Profile view showing rupture direction of events with significant directivity results. Red 'plus' symbols indicate southeast rupture while blue 'open circle' symbols indicate northwest rupture. We overlay a set of arrows indicating rupture directivity of events with $M > 3$. Lighter shaded arrows indicate events in the 2004 aftershock sequence, and the larger gray arrows mark the location and the rupture direction of the 1966 and 2004 mainshocks (not analyzed in this study).

corrections for attenuation within each cluster, and considering resolution capability. Of these results, 243 are significant at the 90% confidence level. We observe a slight preference for rupture directivity toward the southeast for this subset of results with significant estimates, and the proportion of southeast directivity ruptures increases as we limit the data set to increasingly larger earthquakes. These results are consistent with those in two recent studies of rupture directivity at Parkfield, which found that a majority of earthquakes ($1.0 < M < 3.2$ for *Lengliné and Got* [2011]; $0.5 < M < 3.0$ for *Wang and Rubin* [2011]) exhibited southeast rupture directivity.

[36] The bimaterial model that produces asymmetric slip predicts a preference for southeast rupture directivity in the scenario where an interface divides two blocks of different rheological properties. However, the simple model of two blocks separated by a planar fault ignores potentially important heterogeneity of rheological properties on smaller scales, which could modulate the bimaterial effect, and many of the earthquakes considered in this study have rupture diameters (~100–300 m) over which this smaller scale heterogeneity may be important. Imaging studies [e.g., *Thurber et al*., 2006; *Zhao et al*., 2009] additionally resolve variable velocity contrasts along-strike that may contribute to spatial variability of rupture direction.

[37] Our relatively simple approach hides important details when considering the full data set. For example, we observe variability in rupture directivity patterns within spatial groupings of events that could correspond to smaller-scale rheological or stress variability (Figure 6). The 207 $M > 2$ results that do not meet the significance criterion may correspond to ruptures with bilateral or vertical rupture characteristics, or may not have strong enough directivity to be resolved using this method. A recent study of earthquakes at Parkfield performed finite source inversions for a set of small earthquakes and found sizeable vertical rupture components for some ruptures [*Uchide and Ide*, 2010]; our method cannot resolve these features.

[38] Although we note a slight preference for southeast directivity when considering the data set overall and a stronger preference for southeast directivity among larger earthquakes, we observe possible temporal changes in rupture directivity related to the 2004 M 6 Parkfield earthquake. The aftershocks of the 2004 mainshock as well as the subset of $M > 3$ earthquakes following the mainshock contain a higher proportion of events with rupture toward the northwest; this directivity matches the rupture directivity of the mainshock.

[39] In the subset of events $M > 3$, 70% of events exhibited southeast directivity; this differs from the proportion of $M > 4$ events with southeast rupture cataloged by *Harris and Day* [2005]. Southeast rupture directivity is predominant for $M > 3$ events closer to the 1966 earthquake hypocenter yet relatively comparable proportions of both directivities are observed for events closer to the 2004 earthquake hypocenter (Figure 9). This spatial difference is consistent with results from *Lengliné and Got* [2011], in which the proportion of southeast directivity ruptures progressively decreases along-strike and follows the general trend of decreasing material contrast observed by *Zhao et al*. [2009]. Whether the spatial difference in our results is due to such a larger-scale heterogeneity in material contrast or due to temporal effects of the 2004 sequence cannot be easily determined from the limited number of earthquakes analyzed in that section of the fault.

[40] The overall results of our analysis cover a range of possibilities: about half of the estimates $M > 2$ do not produce significant values of directivity (indicating possible vertical or bilateral ruptures), and the remaining half are split between southeast ruptures and northwest ruptures. The degree of variability in apparent rupture direction in a region of seemingly simple geometric fault configuration suggests that there may not be a strong preference for a particular rupture direction over the full range of earthquake magnitudes. The observation of a higher proportion of southeast directivity events for larger magnitude earthquakes is additionally countered by the northwest directivity of the 2004 M 6 Parkfield earthquake. Given the observed spatial variability in results, the possibility of smaller scale controls on rupture directivity due to fault geometry, due to the presence or absence of bimaterial interfaces along-strike, or due to heterogeneous stress distribution cannot be ruled out. The results of this study and other analyses of rupture directivity of earthquakes at Parkfield [e.g., *Harris and Day*, 2005; *Lengliné and Got*, 2011; *Wang and Rubin*, 2011] indicate that rupture directivity is likely due to several contributing factors and that predicting the rupture direction of future earthquakes will be difficult even in regions that appear to have geometrically simple faulting overall.

[41] **Acknowledgments.** Seismic data used in this study was obtained from the Northern California Earthquake Data Center. We thank Debi Kilb for valuable discussions during the completion of this work, and two anonymous reviewers for their helpful comments. This work was supported in part by NSF grant EAR-0908042.

References

Allmann, B. P., and P. M. Shearer (2007), Spatial and temporal stress drop variations in small earthquakes near Parkfield, California, *J. Geophys. Res.*, *112*, B04305, doi:10.1029/2006JB004395.

Andrews, D. J., and R. A. Harris (2005), The wrinkle-like slip pulse is not important in earthquake dynamics, *Geophys. Res. Lett.*, *32*, L23303, doi:10.1029/2005GL023996.

Bakun, W. H., et al. (2005), Implications for prediction and hazard assessment from the 2004 Parkfield earthquake, *Nature*, *437*, doi:10.1038/nature04067.

Ben-Menahem, A. (1961), Radiation of seismic surface-waves from finite moving sources, *Bull. Seism. Soc. Am.*, *51*(3), 401–435.

Ben-Zion, Y. (2006), Comment on "Material contrast does not predict earthquake rupture propagation direction" by R. A. Harris and S. M. Day, *Geophys. Res. Lett.*, *33*, L13310, doi:10.1029/2005GL025652.

Bennington, N., C. Thurber, and S. Roecker (2008), Three-Dimensional Seismic Attenuation Structure around the SAFOD Site, Parkfield, California, *Bull. Seism. Soc. Am.*, *98*(6), 2934–2947.

Boatwright, J. (2007), The persistence of directivity in small earthquakes, *Bull. Seism. Soc. Am.*, *97*(6), 1850–1861, doi:10.1785/0120050228.

Brune, J. (1970), Tectonic stress and the spectra of seismic shear waves from earthquakes, *J. Geophys. Res.*, *75*(26), 4997–5009.

Domanski, B., S. J. Gibowicz, and P. Wiejacz (2002), Source Time Function of Seismic Events at Rudna Copper Mine, Poland, *Pure Appl. Geophys.*, *159*, doi:10.1007/PL00001247.

Eberhart-Phillips, D., and A. Michael (1993), Three-dimensional velocity structure, seismicity, and fault structure in the Parkfield region, central California, *J. Geophys. Res.*, *98*(B9), 15,737–15,758.

Eshelby, J. (1957), The determination of the elastic field of an ellipsoidal inclusion, and related problems, *Proc. Roy. Soc. Lond. Math. Phys. Sci.*, *241*(1226), 376–396.

Fletcher, J. B., P. Spudich, and L. M. Baker (2006), Rupture Propagation of the 2004 Parkfield, California, Earthquake from Observations at the UPSAR, *Bull. Seism. Soc. Am.*, *96*(4B), S129–S142, doi:10.1785/0120050812.

Harris, R. A., and S. M. Day (2005), Material contrast does not predict earthquake rupture propagation direction, *Geophys. Res. Lett.*, *32*, L23301, doi:10.1029/2005GL023941.

Harris, R. A., and S. M. Day (2006), Reply to comment by Y. Ben-Zion on "Material contrast does not predict earthquake rupture propagation direction", *Geophys. Res. Lett.*, *33*(13), L13311, doi:10.1029/2006GL026811.

Hartzell, S. (1978), Earthquake aftershocks as Green's functions, *Geophys. Res. Lett.*, *5*(1).

Haskell, N. (1964), Total energy and energy spectral density of elastic wave radiation from propagating faults, *Bull. Seism. Soc. Am.*, *54*(6), 1811–1851.

Henry, C., and S. Das (2001), Aftershock zones of large shallow earthquakes: fault dimensions, aftershock area expansion and scaling relations, *Geophys. J. Int.*, *147*, 272–293.

Langbein, J., et al. (2005), Preliminary report on the 28 September 2004, M 6.0 Parkfield, California earthquake, *Seism. Res. Lett.*, *76*(1), 10–26.

Lengliné, O., and J.-L. Got (2011), Rupture Directivity of Micro-Earthquake Sequences near Parkfield, California, *Geophys. Res. Lett.*, *38*, L08310, doi:10.1029/2011GL047303.

Lin, G., and P. Shearer (2005), Tests of relative earthquake location techniques using synthetic data, *J. Geophys. Res.*, *110*, B04304, doi:10.1029/2004JB003380.

Lin, G., P. M. Shearer, and E. Hauksson (2007), Applying a three-dimensional velocity model, waveform cross correlation, and cluster analysis to locate southern California seismicity from 1981 to 2005, *J. Geophys. Res.*, *112*, B12309, doi:10.1029/2007JB004986.

Lloyd, S. P. (1982), Least Squares Quantization in PCM, *IEEE Trans. on Information Theory*, *28*(2), 129–137.

Madariaga, R. (1976), Dynamics of an expanding circular fault, *Bull. Seism. Soc. Am.*, *66*(3), 639–666.

Mai, P., P. Spudich, and J. Boatwright (2005), Hypocenter Locations in Finite-Source Rupture Models, *Bull. Seism. Soc. Am.*, *95*(3), 965–980, doi:10.1785/0120040111.

McGuire, J., L. Zhao, and T. Jordan (2002), Predominance of unilateral rupture for a global catalog of large earthquakes, *Bull. Seism. Soc. Am.*, *92*(8), 3309–3317.

Prieto, G., P. M. Shearer, F. L. Vernon, and D. Kilb (2004), Earthquake source scaling and self-similarity estimation from stacking P and S spectra, *J. Geophys. Res*, *109*, B08310.

Rubin, A. (2002), Aftershocks of microearthquakes as probes of the mechanics of rupture, *J. Geophys. Res.*, *107*(B7), 2142, doi:10.1029/2001JB000496.

Rubin, A., and D. Gillard (2000), Aftershock asymmetry/rupture directivity among central San Andreas fault microearthquakes, *J. Geophys. Res.*, *105*(B8), 19,095–19,109.

Shearer, P. M., G. A. Prieto, and E. Hauksson (2006), Comprehensive analysis of earthquake source spectra in southern California, *J. Geophys. Res.*, *111*, B06303, doi:10.1029/2005JB003979.

Shi, Z., and Y. Ben-Zion (2006), Dynamic rupture on a bimaterial interface governed by slip-weakening friction, *Geophys. J. Int.*, doi:10.1111/j.1365-246X.2006.02853.x

Simpson, R. W., M. Barall, J. Langbein, J. R. Murray, and M. J. Rymer (2006), San Andreas Fault Geometry in the Parkfield, California, Region, *Bull. Seism. Soc. Am.*, *96*(4B), S28–S37, doi:10.1785/0120050824.

Thurber, C., H. Zhang, F. Waldhauser, J. Hardebeck, A. Michael, and D. Eberhart-Phillips (2006), Three-Dimensional Compressional Wavespeed Model, Earthquake Relocations, and Focal Mechanisms for the Parkfield, California, *Region, Bull. Seism. Soc. Am.*, *96*(4B), S38.

Uchide, T., and S. Ide (2010), Scaling of earthquake rupture growth in the Parkfield area: Self-similar growth and suppression by the finite seismogenic layer, *J. Geophys. Res.*, *115*, B11302, doi:10.1029/2009JB007122.

Waldhauser, F., W. L. Ellsworth, D. P. Schaff, and A. Cole (2004), Streaks, multiplets, and holes: high-resolution spatio-temporal behavior of Parkfield seismicity, *Geophys. Res. Lett.*, *31*, L18608, doi:10.1029/2004GL020649.

Wallace, R. (1990), The San Andreas Fault System, California, *U.S. Geol. Surv. Prof. Pap.*, *1515*.

Wang, E., and Rubin, A. (2011), Rupture directivity of microearthquakes on the San Andreas fault from spectral ratio inversion, *Geophys. J. Int.*, *186*(2), doi:10.1111/j.1365-246X.2011.05087.x.

Warren, L., and P. Shearer (2002), Mapping lateral variations in upper mantle attenuation by stacking P and PP spectra, *J. Geophys. Res.*, *107*(B12), doi:10.1029/2001JB001195.

Yamashita, T. (2009), Rupture Dynamics on Bimaterial Faults and Nonlinear Off-Fault Damage, in *Fault-Zone Properties and Earthquake Rupture Dynamics, International Geophysics*, Vol. 94, edited by E. Fukuyama, p. 187–215, Elsevier.

Zaliapin, I., and Y. Ben-Zion (2011), Asymmetric distribution of aftershocks on large faults in California, *Geophys. J. Int.*, *185*(3), doi:10.1111/j.1365-246X.2011.04995.x.

Zhao, P., Z. Peng, Z. Shi, M. A. Lewis, and Y. Ben-Zion (2009), Variations of the velocity contrast and rupture properties of M6 earthquakes along the Parkfield section of the San Andreas fault, *Geophys. J. Int.*, *180*(2), doi:10.1111/j.1365-246X.2009.04436.x.